A subset of epithelioid and spindle cell rhabdomyosarcomas is associated with TFCP2 fusions and common ALK upregulation

Francois Le Loarer, Arjen H G Cleven, Corinne Bouvier, Marie-Pierre Castex, Cleofe Romagosa, Anne Moreau, Sebastien Salas, Benjamin Bonhomme, Anne Gomez-Brouchet, Camille Laurent, et al.

A subset of epithelioid and spindle cell rhabdomyosarcomas is associated with *TFCP2* fusions and common ALK upregulation.

F. Le Loarer*123, A.H.G. Cleven*4, C. Bouvier5, MP. Castex6, C. Romagosa7, A. Moreau8, S. Salas9, B. Bonhomme1, A. Gomez-Brouchet10, C. Laurent10, S. Le Guellec10, V Audard11, A Giraud12, I Ramos-Oliver7, A.M Cleton-Jansen4, C.D. Savci-Heijink13, HM Kroon14, J Baud2,3**,** D. Pissaloux15,16, G. Pierron17, A. Sherwood18, JM. Coindre1,2,3, J.V.M.G. Bovée4, F. Larousserie11, F. Tirode16

Authors' names and degrees

Judith V.M.G. BOVEE, MD, PhD

Arjen H.G. CLEVEN, MD, PhD

Marie-Pierre CASTEX, MD

François LE LOARER, MD, PhD

Corinne BOUVIER, MD, PhD

Antoine GIRAUD, MSc

Herman M. KROON, MD, PhD

Irma RAMOS OLIVER, MD

Anne-Marie CLETON-JANSEN, PhD

Dilara C SAVCI-HEIJINK, MD, PhD

Frédérique LAROUSSERIE, MD, PhD

Virginie AUDARD, MD, PhD

Anne GOMEZ- BROUCHET, MD, PhD

Camille LAURENT, MD, PhD

Sophie LE GUELLEC, MD

Jessica BAUD, PhD

Anne MOREAU, MD

Daniel PISSALOUX, PhD

Gaëlle PIERRON, PhD

Anand SHERWOOD, MDS, PhD

Jean Michel COINDRE, MD

Benjamin BONHOMME, MD

Cleofe ROMAGOSA, MD

Sébastien SALAS, MD, PhD

Franck TIRODE, PhD

Authors' affiliations

*These Authors contributed equally

1 Institut Bergonié, Department of Pathology, Bordeaux, France

2 Université de Bordeaux, Talence, France

3 INSERM U1218 ACTION, Institut Bergonie, Bordeaux, France

4 Department of Pathology, Leiden University Medical Center, Leiden, the Netherlands

5 Department of Pathology, Hôpital La Timone, APHM, Marseille, France

6 Department of pediatric oncology, Oncopôle, Toulouse, France

7 Department of Pathology, Vall d'Hebron University Hospital, Barcelona, Spain

8 Department of Pathology, CHU Nantes, Nantes, France

9 Department of Oncology, AP-HM, Marseille, France

10 Department of Pathology, Institut Claudius Regaud-Institut universitaire du cancer-Oncopôle, Toulouse, France

11 Department of Pathology, Hôpital Cochin, APHP, Paris, France

12 Department of clinical trials, Institut Bergonié, Bordeaux, France

13 Department of Pathology, Academic Medical Center, Amsterdam, the Netherlands, Department of

14 Department of Radiology, Leiden University Medical Center, Leiden, the Netherlands.

15 Centre Léon Bérard, Department of Biopathologie, Lyon, France

16 Univ Lyon, Université Claude Bernard Lyon 1, CNRS 5286, INSERM U1052, Cancer Research Center of Lyon, France

17 Institut Curie, Department of biology of tumors, Paris, France

18 Department of Conservative Dentistry and Endodontics, CSI College of Dental Sciences, Madurai, India

Correspondence

Dr François LE LOARER

Telephone: +33 5 47 30 61 85

Fax: +33 5 56 33 04 38

Email : f.le-loarer@bordeaux.unicancer.fr

Running title: *TFCP2* fusions in rhabdomyosarcomas

ABSTRACT

Rhabdomyosarcomas with *TFCP2* fusions represent an emerging subtype of tumors, initially discovered by RNA-sequencing. We report herein the clinicopathological, transcriptional and genomic features of a series of 14 cases.

Cases were retrospectively and prospectively recruited and studied by immunohistochemistry (MYF4, MYOD1, S100, AE1/E3, ALK), fluorescence in situ hybridization with *TFCP2* break-apart probe (n=10/14), array-comparative genomic hybridization (Agilent), whole RNA-sequencing (Truseq Exome, Illumina) or anchored multiplex PCR based targeted next-generation sequencing (Archer® FusionPlex® Sarcoma kit).

Patient's age ranged between 11 to 86 years, including 5 pediatric cases. Tumors were located in bone (n=12/14) and soft tissue (n=2/14). Most bone tumors invaded surrounding soft tissue. Craniofacial bones were over-represented (n=8/12). Median survival was 8 months and 5 patients are currently alive with a median follow-up of 20 months. Most tumors displayed a mixed spindle cell and epithelioid pattern with frequent vesicular nuclei. All tumors expressed keratins and showed a rhabdomyogenic phenotype (defined as expression of MYF4 and/or MYOD1). ALK was overexpressed in all but 3 cases without underlying *ALK* fusion on break-apart FISH (n=5) nor next generation sequencing (n=14). *TFCP2* was fused in 5' either to *EWSR1* (n=6) or *FUS* (n=8). *EWSR1* was involved in both soft tissue cases. FISH with *TFCP2* break-apart probe was positive in all tested cases (n=8), including one case with unbalanced signal. On array-CGH, all tested tumors displayed complex genetic profiles with genomic indexes ranging from 12.8 to 90 and *CDKN2A* deletion was recurrent (n=9/10). *FET-TFCP2* rhabdomyosarcomas clustered together and distinctly from other rhabdomyosarcomas subgroups.

Altogether, our data confirm and expand the spectrum of the new family of *FET-TFCP2* rhabdomyosarcomas which are associated with a predilection for the craniofacial bones, an aggressive course and recurrent pathological features. Their association with ALK overexpression might represent a therapeutic vulnerability.

ORIGINAL ARTICLE

Introduction

Rhabdomyosarcomas belong to a clinically and biologically heterogeneous family of tumors sharing re-expression of immature skeletal muscle differentiation factors, including MYF4/MYOGENIN and/or MYOD1 proteins. They are currently classified into 4 main subtypes: embryonal, alveolar, pleomorphic and spindle cell/sclerosing (1). Nonetheless, recent studies have deciphered the spindle cell/sclerosing family into molecularly distinct subtypes including *NCOA2*-rearranged infantile rhabdomyosarcomas *(2)*, *VGLL2*-rearranged rhabdomyosarcomas (3) and spindle cell/sclerosing rhabdomyosarcomas with *MYOD1* exon 1 mutations (4, 5).

More recently, a new subtype of rhabdomyosarcomas has been identified through a RNA-sequencing screening, defined by *TFCP2* rearrangements (6). These tumors were initially reported as a "new variant of epithelioid rhabdomyosarcomas" and have a striking predilection for bones, especially for the craniofacial skeleton, which is a very uncommon feature for rhabdomyosarcomas (6). Their morphological spectrum has been subsequently extended with the description of cases with spindle cell morphology in the small case series reported so far with a total of 10 cases now described in the literature (7-10). The emerging evidence highlight their predilection for bones, female patients, a frequent spindle cell morphology, common ALK overexpression but substantial clinical follow-up is available for only 2 cases.

We report herein the clinicopathological and molecular features of a series of 14 *FET-TFCP2* rhabdomyosarcomas, highlighting their recurrent morphological and molecular features, paving the way to their diagnosis and recognition in routine practice. Our data confirm that they represent a distinct type of rhabdomyosarcoma.

MATERIAL AND METHODS

Sample selection

Three index cases (TFCP2-1 to 3) were identified through a retrospective RNA-sequencing screening of unclassified sarcomas and were previously reported without detailed clinicopathological data(6). Seven cases were identified prospectively: 6 cases were diagnosed on morphological grounds and 1 case (TFCP2-8) diagnosed on molecular grounds. Control cases were retrieved from the archives of the sarcoma pathology review network (RRePS and Resos) and Institut Bergonie, including malignant peripheral nerve sheath tumors with rhabdomyosarcomatous differentiation (Triton tumor), epithelioid/pleomorphic/embryonal and alveolar rhabdomyosarcomas. All sarcoma cases are recorded in the national sarcoma pathology RREPS and RESOS databases, approved by the National Committee for Protection of Personal Data (CNIL, n°910390), in compliance with ethics principles of the chart of Helsinki. Cases 11-14 were retrieved from the files of A.H.G.C and J.V.M.G.B, including 2 retrospective and 2 prospective cases.

Clinical review

Clinical follow-up was obtained from the medical records of patients provided by participating institutions or through corresponding clinicians. Survival was calculated from the date of diagnosis to the date of death or last date of follow-up. The clinical onset of disease was defined by the first symptom of cancer. Follow-up duration was calculated from the date of the first clinical consultation. clinical management data are provided in **Table 2**. Survival analysis was performed with the Kaplan-Meier method using the dates of initial diagnosis and the dates of death from any cause.

Histopathological analysis

All material (biopsy and surgical specimen if surgery was performed) was centrally reviewed by specialized soft tissue and bone pathologists (FLL, JMC, AHGC, JVMGB).

Immunohistochemistry

The tissue slides were deparaffinized in xylene, hydrated in alcohol, and baked in a microwave (30 min in Trisbuffer, pH 9). Endogenous peroxidase was blocked. Staining was performed on the Benchmark ultra-automated stainer (Ventana) using diamino-benzidine as chromogen (Dako, Glostrup, Denmark). The following antibodies were used: AE1/E3 (clone PCK26, Ventana), KL1 (clone KL1, HISTOLS

reagent), EMA (clone E29, Ventana), P63 (4A4, Ventana), S100 protein (clone poly Z311, Dako), SOX10 (EP268, BioSB), Desmin (clone DE-R11, Ventana), Myogenin (clone LO26, Leica), MYOD1 (clone EP212, Cell marque), ALK (clones D5F3, Cell Signaling Technology and clone 1A4, Novocastra), CD99/MIC2 (12E7, Dako), ETV4 (clone 16, Santa Cruz), CD30 (BerH2, Dako), CD4 4B12, Novocastra), CD7 (SP94, Ventana).

Fluorescence in situ hybridization (FISH)

FISH analyses were performed with 4 μm sections of formalin-fixed paraffin-embedded tissue with the use of Histology FISH Accessory Kit (DAKO, reference : K5799) using commercial break apart probes targeting *EWSR1 (*ZytoLight SPEC *EWSR1* Dual Color Break Apart Probe, Zytovision, reference Z-2096-200), *FUS* (ZytoLight SPEC FUS Dual Color Break Apart Probe, Zytovision, reference Z-2130-50), *ALK* (ZytoLight SPEC ALK Dual Color Break Apart Probe, Zytovision, reference Z-2124-200), *TFCP2* (TFCP2 Break Apart probe, Empire Genomics), reference EG-TFCP2BA-20-GROR). Nuclei were scored for non-rearranged patterns (red and green fusion signals), rearranged and unbalanced patterns (split of red and green signals or extra single red signals) using a Nikon Eclipse 80i fluorescent microscope with appropriate filters. The positive cutoff was ≥20%. Pictures were captured using a Hamamatsu C4742-95 CCD camera and analyzed with the Genikon software (Alphelys).

Array comparative genomic hybridization (a-CGH)

Genomic DNA was extracted from formalin-fixed paraffin-embedded tissue using QIAamp, DNA micro kit (Qiagen, Hilden, Germany). Genomic DNA and human reference DNA (Promega) were labeled with cyanin 5 (Cy5) and cyanin 3 (Cy3), respectively, using the Genomic DNA *ULS* Labeling Kit (Agilent Technologies, Santa Clara, California) and co-hybridized onto a Sureprint G3 Human CGH microarray 4x180K (Agilent) following manufacturer's recommendations. Data were analyzed with Agilent Genomic Workbench software (v7.0, Agilent) or by Cytogenomics software (v2.9.2.4, Agilent). Large-size alterations were defined as quantitative anomalies of whole chromosomes or of segments of chromosomes involving many probes of the array, easily detectable without a specific query on a given

genomic region; Small-size alterations were quantitative anomalies involving only few probes, not detected by the automatic algorithm but after manual analysis of the genomic regions.

Sanger sequencing of *MYOD1*

50ng of FFPE DNA was amplified with forward (AAGCGCAAGACCACCAAC) and reverse primers (GTTGCGCAGGATCTCCAC) targeting exon 1 of *MYOD1*. The PCR products were analyzed by 2% agarose gel electrophoresis with an expected product size of 153 bp. The PCR products were sequenced using a Big Dye Terminator v3.1 Cycle Sequencing Kit (Applied Biosystems, Foster City, CA) on a 3130XL Genetic Analyzer (Applied Biosystems).

Whole RNA-sequencing

RNA-sequencing was performed on formalin-fixed paraffin-embedded material in 10 cases (notably, cases TFCP2 1-3, the three previously reported cases studied by RNA-sequencing on frozen material(6), were re-sequenced with FFPE samples to ensure data comparability).

Total RNA was extracted from formalin-fixed paraffin-embedded tissue section using the Formapure RNA kit (Beckman Coulter, Brea, California) following manufacturers' recommendations. Quantity and quality of total RNA were evaluated using NanoDrop (Thermo Fisher Scientific) and Tape Station with Hs RNA Screen Tape (Agilent) using a cut off of DV_{200} (defined as the percentage of RNA fragments above 200 nucleotides) above 30%. All samples passed quality criteria. Libraries were prepared with 100 ng of total RNA using TruSeq RNA Access Library Prep Kit (Illumina, San Diego, USA). Libraries were pooled by group of 12 samples. Paired-end sequencing was performed using the NextSeq 500/550 High Output V2 kit (150 cycles) on Illumina NextSeq 500 platform (Illumina, San Diego, CA). To perform the clustering analysis, gene expression values were extracted using Kallisto v0.42.5 tool(11) with GENECODE release 23 genome annotation based on GRCh38 genome reference. Kallisto TPM expression values were transformed in log2(TPM+2) and all samples were normalized together using the quantile method from the R limma package within R (version 3.1.1) environment. Clustering was performed with the R package Cluster v2.0.3 ConsensusClusterPlus v 1.46(12) using 1000 permutations

of 80% of both samples and genes. Agnes was used as the clustering algorithm with Pearson correlation distance and Ward's clustering method.

Anchored multiplex PCR

Cases 11 to 14 were analysed only by targeted RNA-sequencing. For the detection of translocations, total nucleic acid was isolated from 5 FFPE slides of 10 µm using the Tissue Preparation System (Siemens) after microdissection. After measurement of RNA quantity for FFPE material with Qubit fluorometric quantification system (Life Technologies), the target-enriched cDNA library was prepared with the Archer® FusionPlex® Sarcoma kit as per manufacturer's description. As described previously (13) , reverse transcription of RNA was followed by end repair, adenylation and universal half-functional adapter ligation of double-stranded cDNA fragments. This was followed by two rounds of low cycle PCR with universal primers and gene specific primers, covering 26 target genes that rendered the library fully functional for clonal amplification and sequencing using the Ion Proton™ or the Ion S5™ system. With the Archer analysis software (version 5.0) the produced libraries were analyzed for presence of relevant fusions. Sequence quality was assessed by the following criteria: QC score of <30, a minimal total read number of 1.5 million with >7% unique fragments and >40% RNA reads.

RESULTS

Clinical, radiological and macroscopic findings

The age at diagnosis ranged from 11 to 86 years with a mean of 31 years (**Table 1**). There were 5 pediatric patients (defined as less than 18 years of age) and a slight female predominance was seen (8 female vs 6 male patients).

Tumor size ranged from 20 to 150 mm with a median size of 60 mm. Tumors were most often located in bones (n=12/14) or soft tissue (n=2/14). Bone tumors presented at locally advanced stage (**Figures 1, 3, 4 and 5),** invading surrounding tissues in all but one case (n=11/12). Two cases involved two contiguous bones (n=2/12). In one case, the tumor was bifocal within femoral bone (case TFCP2-7). Involved bones included the cranial bones (n=3), bones of the orofacial complex (n=6, mandible being the most commonly affected bone), vertebra, long bone and sacrum (1 case each). When performed,

gross examination confirmed, in case of bone origin, destruction of cortical bone and extension in surrounding soft tissue (**Supplementary Figure 1**). Regarding soft tissue tumors, locations included the peritoneum and inguinal area (the origin and precise level of extension of this case were not available, TFCP2-6).

Overall, all patients received chemotherapy with varied regimens, including 2 patients with neoadjuvant chemotherapy and 4 patients with chemotherapy as the sole therapeutic modality (**Table 2**). No consistent therapeutic response was achieved with conventional chemotherapy. Other treatment modalities included surgery (n=7). Local control was achieved with surgery in 6 patients, including 2 R1 micro surgery (i.e. defined as the presence of microscopic tumor residue) and 4 R0 surgery but local relapse occurred in all patients (**Table 2).** Seven patients had metastatic disease, either at presentation (n=3/14) or at follow-up (n=4/14). Metastases involved lungs (n=6/7), bones (n=2/7) and lymph nodes (n=1/7).

The mean survival was 8 months. The cohort included 8 patients dead of disease and 5 patients alive, of whom 2 had evidence of clinical progression (**Tables 1 and 2**). The probability of survival was estimated to 46% at 12 months with Kaplan Meier analysis (**Supplementary Figure 2**). Among alive patients in this series (n=5), all but one had undergone radical surgery and the mean follow-up was 6 months, with two patients currently in clinical progression. The sole survivor without surgery had unresectable tumor which was progressive despite combined VDC-IE chemotherapy and radiation therapy and was subsequently switched to targeted therapy (Alectinib) which halted progression (slight tumor regression from 53x27 to 32x29 mm) at 7mo of therapy (**Table 2**, TFCP2-8).

Microscopic findings

Tumors had been initially heterogeneously classified with diagnosis of spindle cell rhabdomyosarcoma (n=3), epithelioid rhabdomyosarcoma (n=2), embryonal and unclassified rhabdomyosarcomas not otherwise specified (NOS) (n=2 and 2, respectively), malignant Triton tumor (n=2), desmoplastic small round cell tumor (n=1), unclassified sarcoma with a spindle cell phenotype (n=1) and anaplastic lymphoma (n=1) (**Table 3**).

Most tumors (n=9/14) showed a hybrid spindle cell and epithelioid cytomorphology (**Figure 1B-D**) while the other cases had essentially epithelioid (n=3) (**Figures 2A-B**), round cell (n=1) (**Figures 2C-D**) or spindle cell morphology (**Figure 3B-C)**.

The lesional cells had abundant eosinophilic cytoplasm and oval nuclei dotted with distinct nucleoli in most cases (n=9/14) (**Figure 4E**). Nuclear hyperchromasia and pleomorphism (defined as variations in size and shape of the nuclei) were focally seen in 4 cases (**Figures 2F**). Scattered rhabdomyoblasts were seen in 2 cases (n=2/14) (**Figure 5F**). There was no significant stroma in half of the cases but focal fibrous changes were seen in 6 cases (**Figure 2E**). A single case displayed a diffuse hyalinized stroma that encased the tumor cells, accounting for a trabecular growth pattern (**Figures 2C-D)**. Tumor necrosis was present in all but two tumors (**Table 3**)."

Immunohistochemical findings

All but one case expressed desmin either diffusely (n=8/14), heterogeneously (n=3/14) or only focally (n=2/14). All tumors expressed either MYOD1 or myogenin. MYOD1 was strongly expressed (i.e.>50%) in all but three cases (n=11/14) while myogenin staining was only focally (<35%) positive in most cases (n=9/14), negative in 3 cases (n=3/14) and diffusely positive in 2 cases (**Table 3, Figure 1**). Notably, MYOD1 was diffusely positive in all tumors negative for myogenin. Keratins AE1/E3 were positive in all cases (n=14), with focal staining in 4 cases (**Figures 1 and 4**). ALK was overexpressed in all but 3 cases, with diffuse cytoplasmic overexpression (>50%) in all positive cases (**Figures 1, 4 and 5)**. In one case, CD30 and CD4 were focally positive, accounting for its initial misdiagnosis as anaplastic lymphoma but no significant staining was seen in other tested cases (n=8). S100 protein was focally positive in 6 cases and diffusely positive in 1 case, without concomitant expression of SOX10 in tested cases (n=0/10).

Fluorescence in situ hybridization

EWSR1 break-apart FISH was positive in all but one *EWSR1-TFCP2* tumors (n=2/3), including one case with 3' loss, consistent with unbalanced translocation (**Supplementary Table3**). Break-apart FISH for *FUS* was positive in all tested cases (n=5/5).

No rearrangement of *ALK* was seen nor by a FISH break part assay for *ALK* (n=0/5) nor by RNA-sequencing (n=0/14) (**Supplementary Table 1**).

FISH with *TFCP2* break-apart probe was positive in all tested case (n=9) (**Figures 3 and 4**), including one case with an unbalanced split signal. To test the specificity of *TFCP2* rearrangements in the setting of rhabdomyosarcomas, we tested 31 cases of rhabdomyosarcomas spanning the different subtypes by break-apart FISH with a break-apart probe for *TFCP2* (**Supplementary Table 2**). All control cases were negative for rearrangement, including 4 sporadic malignant triton tumors, 1 Neurofibromatosis type 1-associated malignant triton tumor, 10 pleomorphic rhabdomyosarcomas, 1 case each of embryonal rhabdomyosarcoma and alveolar rhabdomyosarcoma; 3 spindle cell rhabdomyosarcomas, 9 cases of epithelioid rhabdomyosarcomas, 1 case of carcinoma with rhabdomyosarcomatous component and 2 cases of unclassified sarcomas with epithelioid phenotype (**Supplementary Table 2**).

Array-comparative genomic hybridization and *MYOD1* mutational analysis

Mutations in the exon 1 of *MYOD1* were absent at DNA level (n=0/8) as well as RNA level (n=0/10) (**Supplementary Table 1**).

Genomic profiling was performed in 10 cases, showing overall rearranged profiles with high genomic index ranging from 13.5 to 107.55. Two *EWSR1-TFCP2* tumors (n=2/4) and one *FUS-TFCP2* tumor (n=1/5) displayed genomic breakpoints within *EWSR1* and *FUS* loci, respectively. Two tumors had a genomic breakpoint within *TFCP2* locus. All cases displayed homozygous deletion of the tumor suppressor gene *CDKN2A* (n=9/9) **(Supplementary Table 3, Figure 4).** Two cases displayed additional homozygous deletions spanning in the first case: *PRKAR2A* in 3p21.31, *AUTS2* in 7q11.22, *PTPN12* in 7q11.23-q21.11, *PDE3A* in 12p12.2, *ST8SIA1* in 12p21.1, *LARGE1* in 22q12.3 and in the second case *MAP3K15*, *GPR63* and *PHKA2* in Xp22.13-p22.12 and the locus 16p11.2-q12.1. Genomic amplifications were seen in one case spanning most notably *MDM2* in 12q15, *CCNE1* in 19q12-q13.11, and *MAP3K1* in 5q11.2-12.1. Focusing on *ALK* locus**,** five cases displayed alterations (n=5/9), including an internal hemizygous deletion in 3 cases, a hemizygous deletion and a homozygous internal deletion in one case each.

RNA-sequencing findings

Whole RNA-sequencing was performed on FFPE material in 10 cases and 4 cases were studied by Anchored multiplex PCR (**Supplementary Table 1**). Four cases of this series, including the three index

cases of *FET-TFCP2* rhabdomyosarcomas, were diagnosed based on RNA-sequencing findings without prior pathological suspicion of the diagnosis. *TFCP2* was either fused to *FUS* (n=8) or to *EWSR1* (n=6). Breakpoints involved constantly exon 2 of *TFCP2*, exons 5 or 6 of *FUS* and *EWSR1*. The transcriptomes of the 7 cases sequenced on the same whole RNA-sequencing platform were compared with embryonal rhabdomyosarcomas (n=6), alveolar rhabdomyosarcoma (n=8), *MYOD1*-mutated rhabdomyosarcomas (n=4) and *VGLL2*-fused rhabdomyosarcomas (n=5). Unsupervised consensus clustering analyses highlighted that these 7 *FET-TFCP2* samples clustered apart from the other rhabdomyosarcomas (**Supplementary Figure 3**). Expression analysis evidenced *ALK* RNA upregulation in all but 2 samples available for analysis (n=10). These 2 cases were notably negative for ALK in immunohistochemistry. *ALK* transcripts upregulation in *FET-TFCP2* rhabdomyosarcomas was at least at the level of *ALK*-rearranged inflammatory myofibroblastic tumors or *ALK*-rearranged Spitz nevi (**Supplementary Figure 3**). No fusion involving *ALK* was identified by targeted or whole transcriptome sequencing. At transcriptional level, *ALK* upregulation was stronger in the subset of tumors associated with genomic deletion of *ALK* and was uneven along the transcript. The upregulation predominated on the sequences beyond exon 17, a finding which has been found in case of alternative transcription initiation (14) (**Supplementary Figure 4X**).

Fusions were characterized by anchored multiplex PCR in 4 cases, showing 2 cases each of *FUS-TFCP2* and *EWSR1-TFCP2* fusions, involving the same exons than those seen in the cohort explored by RNA-sequencing (**Table 1**).

DISCUSSION

Rhabdomyosarcomas represent a clinically and biologically heterogeneous group of tumors that share by definition the re-expression of the immature myogenic markers Myogenin and MYOD1(15). However, rhabdomyosarcomatous differentiation can be seen in many tumor types both epithelial with the example of carcinosarcomas(16) and mesenchymal malignancies, including malignant Triton tumors, biphenotypic sinonasal sarcomas(17) mesenchymal chondrosarcomas(18). The most well-defined categories of rhabdomyosarcomas are those associated with recurrent molecular alterations, which include alveolar rhabdomyosarcoma underlined by *FOXO1* fusions(19), *MYOD1*-mutated spindle cell rhabdomyosarcomas(4, 5), *NCOA2*- and *VGLL2*-fused spindle cell rhabdomyosarcomas(2, 3). The identification of new recurrent molecular features may be helpful to break down the heterogeneous category of spindle cell rhabdomyosarcomas into homogeneous and clinically more accurate subtypes. Our initial description of *FET-TFCP2* rhabdomyosarcomas (6) has hence been followed by the

description of 7 additional cases to date, (6-8, 10, 20) (**Table 4**). Our series report 11 additional cases and provides a comprehensive clinical, pathological, genomic and transcriptional characterization of this emerging entity.

Clinically, *FET-TFCP2* rhabdomyosarcomas display a striking bone predilection with only two cases exclusively located in soft tissue in this series (**Table 1**) while no other soft tissue case is reported in the literature. Most bone cases destroyed the cortex and invaded surrounding soft tissue (**Table 2**). Most intriguingly, craniofacial bones are the commonest bones affected (n=14/18). This is in keeping with available literature of intra-osseous rhabdomyosarcomas as despite their extreme rarity, most published series are available in craniofacial bones, although without molecular characterization of the cases (21, 22). Our data confirm that *FET-TFCP2* tumors mostly affect young adult patients with a median age at diagnosis of 31 years with a slight female predominance (n=13/21). Regarding outcomes, our series provides the best detailed clinical follow-up so far, with a median survival of 8 months. Among patients still alive, 2 have evidence of progressive disease (n=2/5) despite the administration of multimodal therapy (**Table 2**) with available median follow-up of 20 months. Altogether, our series highlights the aggressive behaviour of this entity.

Microscopically, in addition to our initial report, most *FET-TFCP2* rhabdomyosarcomas actually display a hybrid spindle cell and epithelioid pattern. All tumors displayed high grade features with vesicular nuclei, high mitotic activity and tumor necrosis. A rhabdomyosarcomatous immunophenotype was always present, MYOD1 being more sensitive than Myogenin **(Table 3)**. At transcriptional level, *FET-TFCP2* tumors expressed high levels of skeletal muscle transcripts, especially *sarcoglycan alpha*, *MYOD1* and *MYOG(6)*. All tumors consistently expressed keratins. Keratins are commonly expressed in rhabdomyosarcomas (staining was seen in 50% of alveolar rhabdomyosarcoma of our control cohort, **Supplementary Table 4**) although only focally, contrasting with the diffuse expression displayed by most *FET-TFCP2* rhabdomyosarcomas (**Table 3**). Among the other published cases, one case with *FUS-TFCP2* fusion is a "phenotypic outlier", displaying a full myogenic profile (coexpression of caldesmon and SMA) and negative for keratins(10).

These tumors differ from the so-called “epithelioid rhabdomyosarcomas” which display a pure solid architecture, a rare feature in *FET-TFCP2* tumors with only three purely epithelioid cases in this series(23). Moreover, reported cases of epithelioid rhabdomyosarcomas are located in deep soft tissue and scarcely express epithelial markers contrasting with the features of *FET-TFCP2* rhabdomyosarcomas (23). In the control cohort, all 9 epithelioid rhabdomyosarcomas in soft tissue were negative for *TFCP2* rearrangement by FISH break-apart assay, further supporting this pathological subtype is distinct from *FET-TFCP2* rhabdomyosarcomas (**Supplementary Table 2)**. We also report herein a new pattern in *FET-TFCP2* rhabdomyosarcoma with one case associated with a round cell pattern, in which tumor cells were arranged in trabeculae and embedded in an abundant fibromyxoid stroma (**Figure 2C-D**).

All cases were associated with *Transcription Factor Cellular Promoter 2* (*TFCP2*) rearrangements, fused in 5’ to *FUS* (n=8/14) or *EWSR1* (n=6/14). *TFCP2*, also known as *Late Simian Virus 40 factor* (*LSF*), located in 12q13.12 encodes an evolutionarily conserved transcription factor that targets the thymidylate synthase gene, involved in the enzymatic regulation of DNA synthesis(24, 25). TFCP2 contains a N-terminal DNA-binding domain and a C-terminal sterile alpha motif domain involved in protein dimerization (26) *TFCP2* has been formerly linked to cancer with evidence of oncogenic deregulation in hepatocellular carcinoma (27) mediated by C-MET signaling(28). Breakpoints within *TFCP2* occur before the 2nd exon, thereby preserving the DNA binding domain of the protein. This fusion provides a further illustration of alternative involvement of *EWSR1* or *FUS* in a single tumor entity as these 2 genes are structurally and functionally related(29).

Our data show that *FET-TFCP2* rhabdomyosarcomas are associated with overall complex genetic profiles. This is in agreement with the features reported in one case characterized by genomic profiling (Affymetrix platform) which showed a tetraploid profile with numerous alterations, chromotripsis of 1p and 3p and homozygous deletion of *CDKN2A*(20). *CDKN2A* inactivation was indeed seen in all tested cases of our series (**Supplementary Table 3**). Concomitantly, 3 cases had genomic features consistent with unbalanced translocation.

Despite their complex genomic rearrangements, the *FET-TFCP2* rhabdomyosarcomas are transcriptionally homogeneous as they clustered altogether. Moreover, adding more *FET-TFCP2* samples to the initial clustering analyses strengthen their clustering away from the other rhabdomyosarcoma subtypes, as shown by the clear consensus clustering (**Supplementary Figure 3**).

In this series, all but 3 *FET-TFCP2* rhabdomyosarcomas overexpressed ALK both at transcriptional and protein levels, without underlying *ALK* fusion. According to RNA-sequencing and CGH data, this upregulation does not involve translocation nor amplification but correlated with ALK genomic deletion, presumably involving alternative transcription initiation(14) (**Supplementary Figure 4X**). No copy number alteration of *ALK* could be detected in both FET-TFCP2 tumors negative for ALK by immunohistochemistry. Interestingly, *ALK* deletion has been previously reported in one case of *FUS-TFCP2* sarcoma: the sequencing data showed that the upregulation did not involve exons 1-16, therefore in keeping with our finding (20).

Intriguingly, the expression of ALK has been shown with variable frequencies in other types of rhabdomyosarcomas, especially the alveolar subtype in up to 69% of cases (30, 31) but its underlying biological mechanism remains elusive. We confirmed this finding in our control cohort as ALK staining was seen in 88.9% and 28.6% of alveolar and embryonal rhabdomyosarcomas, respectively (**Supplementary Table 4**). Nonetheless, ALK expression is rare in spindle cell rhabdomyosarcomas, present only in 23% of our control cases (**Supplementary Table 4**). Despite ALK overexpression, targeted therapy against ALK has not shown *in vivo* effects nor clinical benefits in alveolar rhabdomyosarcomas patients (32, 33), although the actual levels of expression of ALK were not reported in the studies. It is notable that at transcriptional level, the intensity of *ALK* upregulation is at least as high as in *ALK*-rearranged tumor types, such as *ALK*-fused inflammatory myofibroblastic tumors. Interestingly, one prospective patient of this series benefited from an ALK inhibitor after clinical progression under conventional chemotherapy, which stabilized tumor size with available follow-up of 7 months under therapy (**Table 2**). Therefore, the potential benefits of ALK inhibition in *FET-TFCP2* rhabdomyosarcoma need to be further addressed, either as single therapy or in combination.

FET-TFCP2 rhabdomyosarcomas should not be confused with sarcomas with *EWSR1-PATZ1* fusions as these tumors may develop in bones and display a rhabdomyogenic phenotype (34). The latter tumors have a hybrid spindle cell to round cell phenotype but lack the epithelioid and high grade nuclear features of most *FET-TFCP2* rhabdomyosarcomas. FET-TFCP2 tumors, especially those that have an exclusive spindle cell morphology, may be confused with inflammatory myofibroblastic tumors. Both tumor types commonly express keratins and ALK. Nonetheless, ALK overexpression in inflammatory myofibroblastic tumors is related to underlying *ALK* fusion with a variety of partner genes, in contrast with *FET-TFCP2* rhabdomyosarcomas. Intraosseous rhabdomyosarcomas with *MEIS1-NCOA2* fusions represent another emerging entity with only 2 cases reported for now (8). This variant displays pure spindle cell morphology and does not express keratins nor ALK (8). The rhabdomyogenic phenotype and focal staining for S100 protein seen in a subset of cases may also raise suspicion for a malignant Triton tumor although none of *TFCP2* patients had an underlying neurofibromatosis condition and the SOX10 marker was negative in all tested cases. Furthermore, we did not find *TFCP2* fusions in control cases of malignant triton tumors (**Supplementary Table 2**).

In short, we report herein the largest and most comprehensive study of *FET-TFCP2* rhabdomyosarcomas. This new entity is associated with hybrid epithelioid and spindle cell features, a predilection for craniofacial bones and expresses consistently keratins and ALK. Tumors harboring these features should therefore benefit from molecular investigations seeking for a *FET-TFCP2* fusion gene. Altogether, the clinical, morphological and molecular data strongly suggest that these tumors represent a distinct rhabdomyosarcoma subtype.

Acknowledgements: We are grateful to pathologists and clinicians for sharing cases and follow-up informations: Dr A Al Bouzidi (Rabat, Marocco), Dr E Angot (CHU Rouen), Dr Foucard (Paris), Pr C. Berger (HEGP, Paris), Dr N Bennani Guebessi (Casablanca, Marocco), Dr C Bazille (CHU Caen), Pr F. Gouin (CHU Nantes), Dr E Bompas (ICO, St Herblain), Dr Haffadi (Casablanca), Dr C. Raban (CHU Poitiers), Dr V. Laurence (Institut Curie, Paris), Dr A Moreau (CHU Nantes, France), Dr S Watson (Institut Curie, Paris, France), Prof D. Baumhoer (Basel, Switzerland), Dr M. Chan (Paramaribo, Suriname) and Dr U. Flucke (Nijmegen, Netherlands). Dr A de La Fouchardière (Centre Leon Berard,

Lyon, France) graciously provided the *ALK*-fusion positive Spitz nevi for the transcriptional analysis. The authors thank L Mayeur, V. Velasco and V Fouqué for their assistance. INSERM U1218 is supported by a charity funding “Le Fil d’Oriane”.

Disclosures: The authors have no conflict of interest to declare.

Supplementary information is available at *Modern Pathology’s* website.

REFERENCES

1. Barr F.G., Montgomery E.A., Nascimento A.F., Parham D.M. Skeletal-muscle tumours. In: Fletcher CDM, Bridge J.A., Hogendoorn P.C.W., Mertens F., editors. WHO classification of tumours of soft tissue and bone. 4th ed. Lyon: IARC press, 2013. p.124-135.

2. Mosquera JM, Sboner A, Zhang L, Kitabayashi N, Chen CL, Sung YS *et al.* Recurrent NCOA2 gene rearrangements in congenital/infantile spindle cell rhabdomyosarcoma. Genes Chromosomes Cancer 2013;52:538-50.

3. Alaggio R, Zhang L, Sung YS, Huang SC, Chen CL, Bisogno G *et al.* A Molecular Study of Pediatric Spindle and Sclerosing Rhabdomyosarcoma: Identification of Novel and Recurrent VGLL2-related Fusions in Infantile Cases. Am J Surg Pathol 2016;40:224-35.

4. Kohsaka S, Shukla N, Ameur N, Ito T, Ng CK, Wang L *et al.* A recurrent neomorphic mutation in MYOD1 defines a clinically aggressive subset of embryonal rhabdomyosarcoma associated with PI3K-AKT pathway mutations. Nat Genet 2014;46:595-600.

5. Szuhai K, de Jong D, Leung WY, Fletcher CD, Hogendoorn PC. Transactivating mutation of the MYOD1 gene is a frequent event in adult spindle cell rhabdomyosarcoma. J Pathol 2014;232:300-7.

6. Watson S, Perrin V, Guillemot D, Reynaud S, Coindre JM, Karanian M *et al.* Transcriptomic definition of molecular subgroups of small round cell sarcomas. J Pathol 2018;245:29-40.

7. Dashti NK, Wehrs RN, Thomas BC, Nair A, Davila J, Buckner JC *et al.* Spindle cell rhabdomyosarcoma of bone with FUS-TFCP2 fusion: confirmation of a very recently described rhabdomyosarcoma subtype. Histopathology 2018;73:514-20.

8. Agaram NP, Zhang L, Sung YS, Cavalcanti MS, Torrence D, Wexler L *et al.* Expanding the Spectrum of Intraosseous Rhabdomyosarcoma: Correlation Between 2 Distinct Gene Fusions and Phenotype. Am J Surg Pathol 2019;43:695-702.

9. Tagami Y, Sugita S, Kubo T, Iesato N, Emori M, Takada K, *et al.* Spindle cell rhabdomyosarcoma in a lumbar vertebra with FUS-TFCP2 fusion. Pathol Res Pract 2019; doi: 10.1016/j.prp.2019.03.027 (Epub).

10. Zhu G, Benayed R, Ho C, Mullaney K, Sukhadia P, Rios K, *et al.* Diagnosis of known sarcoma fusions and novel fusion partners by targeted RNA sequencing with identification of a recurrent ACTB-FOSB fusion in pseudomyogenic hemangioendothelioma. Mod Pathol 2018;32:609-620.

11. Bray NL, Pimentel H, Melsted P, Pachter L. Near-optimal probabilistic RNA-seq quantification. Nat Biotechnol 2016;34:525-7.

12. Wilkerson MD, Hayes DN. ConsensusClusterPlus: a class discovery tool with confidence assessments and item tracking. Bioinformatics 2010;26:1572-3.

13. Lam SW, Cleton-Jansen AM, Cleven AHG, Ruano D, van Wezel T, Szuhai K, Bovée JVMG. Molecular Analysis of Gene Fusions in Bone and Soft Tissue Tumors by Anchored Multiplex PCR-Based Targeted Next-Generation Sequencing. J Mol Diagn 2018;20:653-63.

14. Wiesner T, Lee W, Obenauf AC, Ran L, Murali R, Zhang QG *et al.* Alternative transcription initiation leads to expression of a novel ALK isoform in cancer. Nature 2015;526:453-7.

15. Agaram NP. Update on Myogenic Sarcomas. Surg Pathol Clin 2019;12:51-62.

16. McCluggage WG. A practical approach to the diagnosis of mixed epithelial and mesenchymal tumours of the uterus. Mod Pathol 2016;29 Suppl 1:S78-91.

17. Le Loarer F, Laffont S, Lesluyes T, Tirode F, Antonescu C, Baglin AC *et al.* Clinicopathologic and Molecular Features of a Series of 41 Biphenotypic Sinonasal Sarcomas Expanding Their Molecular Spectrum. Am J Surg Pathol 2019, doi: 10.1097/PAS.0000000000001238 (Epub).

18. Folpe AL, Graham RP, Martinez A, Schembri-Wismayer D, Boland J, Fritchie KJ. Mesenchymal chondrosarcomas showing immunohistochemical evidence of rhabdomyoblastic differentiation: a potential diagnostic pitfall. Hum Pathol 2018; 77:28-34.

19. Galili N, Davis RJ, Fredericks WJ, Mukhopadhyay S, Rauscher FJ, Emanuel BS *et al.* Fusion of a fork head domain gene to PAX3 in the solid tumour alveolar rhabdomyosarcoma. Nat Genet 1993;5:230-5.

20. Wong DD, van Vliet C, Gaman A, Giardina T, Amanuel B. Rhabdomyosarcoma with FUS re-arrangement: additional case in support of a novel subtype. Pathology 2019;51:116-20.

21. Iatrou I, Theologie-Lygidakis N, Schoinohoriti O, Tzermpos F, Vessala AM. Rhabdomyosarcoma of the maxillofacial region in children and adolescents: Report of 9 cases and literature review. J Craniomaxillofac Surg 2017;45:831-838.

22. Lucas DR, Ryan JR, Zalupski MM, Gross ML, Ravindranath Y, Ortman B. Primary embryonal rhabdomyosarcoma of long bone. Case report and review of the literature. Am J Surg Pathol 1996;20:239-44.

23. Jo VY, Mariño-Enríquez A, Fletcher CD. Epithelioid rhabdomyosarcoma: clinicopathologic analysis of 16 cases of a morphologically distinct variant of rhabdomyosarcoma. Am J Surg Pathol 2011;35:1523-30.

24. Veljkovic J, Hansen U. Lineage-specific and ubiquitous biological roles of the mammalian transcription factor LSF. Gene 2004;343:23-40.

25. Swendeman SL, Spielholz C, Jenkins NA, Gilbert DJ, Copeland NG, Sheffery M. Characterization of the genomic structure, chromosomal location, promoter, and development expression of the alpha-globin transcription factor CP2. J Biol Chem 1994;269:11663-71.

26. Kotarba G, Krzywinska E, Grabowska AI, Taracha A, Wilanowski T. TFCP2/TFCP2L1/UBP1 transcription factors in cancer. Cancer Lett. 2018;28:72-79.

27. Yoo BK, Emdad L, Gredler R, Fuller C, Dumur Cl, Jones KH *et al.* Transcription factor Late SV40 Factor (LSF) functions as an oncogene in hepatocellular carcinoma. Proc Natl Acad Sci U S A 2010;107:8357-62.

28. Yoo BK, Gredler R, Chen D, Santhekadur PK, Fisher PB, Sarkar D *et al.* c-Met activation through a novel pathway involving osteopontin mediates oncogenesis by the transcription factor LSF. J Hepatol 2011;55:1317-24.

29. Luo Y, Blechingberg J, Fernandes AM, Li S, Fryland T, Borglum AD *et al.* EWS and FUS bind a subset of transcribed genes encoding proteins enriched in RNA regulatory functions. BMC Genomics 2015;16:929.

30. Yoshida A, Shibata T, Wakai S, Ushiku T, Tsuta K, Fukayama M *et al.* Anaplastic lymphoma kinase status in rhabdomyosarcomas. Mod Pathol 2013;26:772-81.

31. Pillay K, Govender D, Chetty R. ALK protein expression in rhabdomyosarcomas. Histopathology 2002;41:461-7.

32. Wierdl M, Tsurkan L, Chi L, Hatfield MJ, Tollemar V, Bradley C *et al.* Targeting ALK in pediatric RMS does not induce antitumor activity in vivo. Cancer chemother Pharmacol 2018;82:251-63.

33. Schoffski P, Wozniak A, Leahy MG, Aamdal S, Rutkowski P, Bauer S *et al.* The tyrosine kinase inhibitor crizotinib does not have clinically meaningful activity in heavily pre-treated patients with advanced alveolar rhabdomyosarcoma with FOXO rearrangement: European Organisation

for Research and Treatment of Cancer phase 2 trial 90101 'CREATE'. Eur J Cancer 2018;94:156-67.

34. Chougule A, Taylor MS, Nardi V, Chebib I, Cote GM, Choy E, *et al.* Spindle and Round Cell Sarcoma With EWSR1-PATZ1 Gene Fusion: A Sarcoma With Polyphenotypic Differentiation. Am J Surg Pathol. 2019;43:220-228.

FIGURE LEGENDS

Figure 1 Typical case of *FET-TFCP2* rhabdomyosarcoma. MR image demonstrating an expansive and destructive mass of the occipital bone in a 31yo male (A, TFCP2-9). The proliferation was arranged in solid sheets (B) and fascicles (C). Tumor cells displayed middle-sized nuclei with distinct nucleoli and mild anisocaryosis along with abundant eosinophilic cytoplasm (D). Cells stained focally for Myogenin (E), diffusely for MYOD1 (F) and diffusely for ALK (G). Cytokeratins AE1/3 and Desmin were heterogeneously and diffusely expressed, respectively (not shown).

Figure 2 Morphological variants seen in *FET-TFCP2* rhabdomyosarcomas. Three *FET-TFCP2* cases displayed pure epithelioid cytomorphology where tumor cells are arranged in solid sheets (A, case TFCP2-2) and harboured abundant globoid eosinophilic cytoplasm (B). One case of *FET-TFCP2* rhabdomyosarcoma **(**TFCP2-8) displayed more abundant fibrous and myxoid stromal changes than seen in other cases (C) and tumor cells displayed small to medium rounded nuclei with fine chromatin without nucleoli (D). This tumor was associated with a *FUS-TFCP2* fusion and displayed otherwise similar immunophenotypic and RNA expression features to other *FET-TFCP2* tumors. *FET-TFCP2* rhabdomyosarcomas may focally display fibrous stromal changes (E). Tumor nuclei were mostly monomorphic while a subset of cases harboured marked anisokaryosis with variations in size and shape of the nuclei and conspicuous mitotic activity (F).

Figure 3 Case of *FET-TFCP2* rhabdomyosarcoma with pure spindle cell moprhology. CT of an osteolytic lesion of the mandible with cortical destruction and soft-tissue extension (A, TFCP2-10). Tumor cells were arranged in intersecting fascicles with abundant eosinophilic cytoplasm (B, C). Tumor cells expressed heterogeneously desmin (D) and diffusely MYOD1 (E). Tumors cells displayed a split signal by FISH with the *TFCP2* break-apart probe (F).

Figure 4 Case of *FET-TFCP2* rhabdomyosarcoma with small nuclear cytomorphology. CT of a multifocal osteolytic lesion of the right femur in the intertrochanteric area and femoral neck (A, B coronal reformatted and axial views, respectively) (case TFCP2-7). Core-needle biopsy evidence a mixed proliferation arranged in short fascicles (C) and solid sheets (D). Tumor cells harbor ovoid nuclei with fine chromatin without nucleoli, relatively monomorphic (E). The proliferation stained diffusely for ALK (F), AE1/3 (G) and MYOD1 (H). A split signal is seen with the FISH assay using a break-apart probe spanning *TFCP2* (I). array-comparative genomic hybridization evidenced copy number alterations across the genome including homozygous deletion of *CDKN2A* and breakpoint within *EWSR1* locus, in keeping with the presence of an underlying *EWSR1-TFCP2* fusion (J).

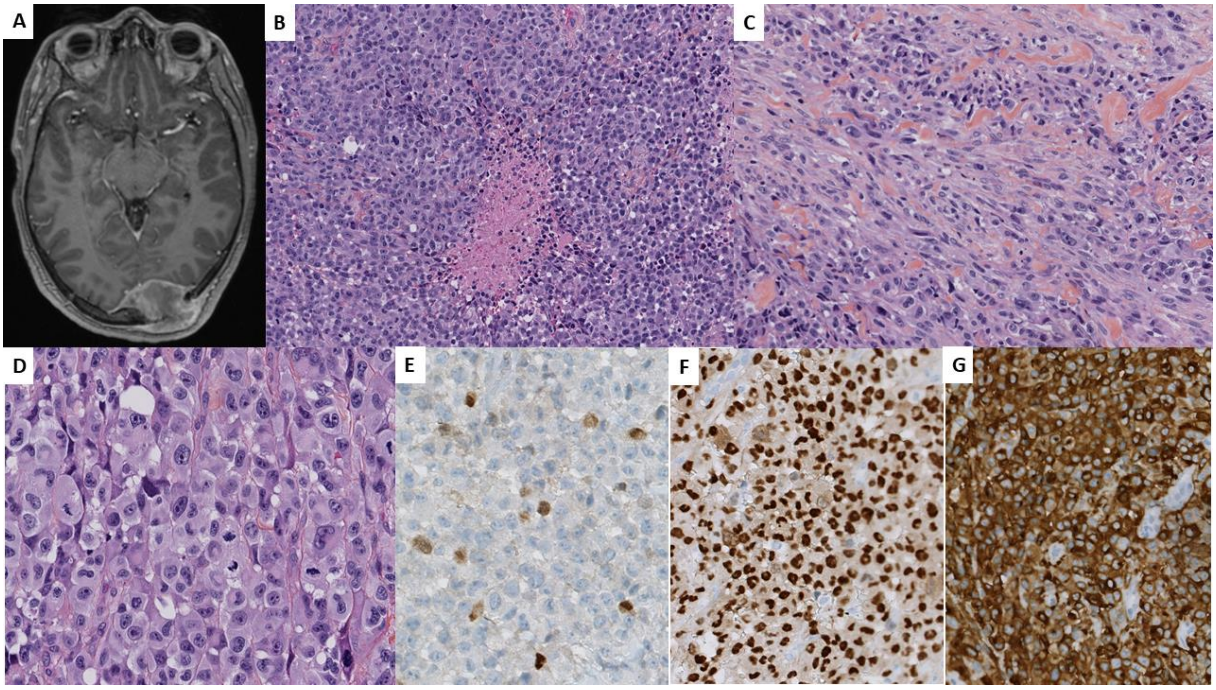

Figure 1

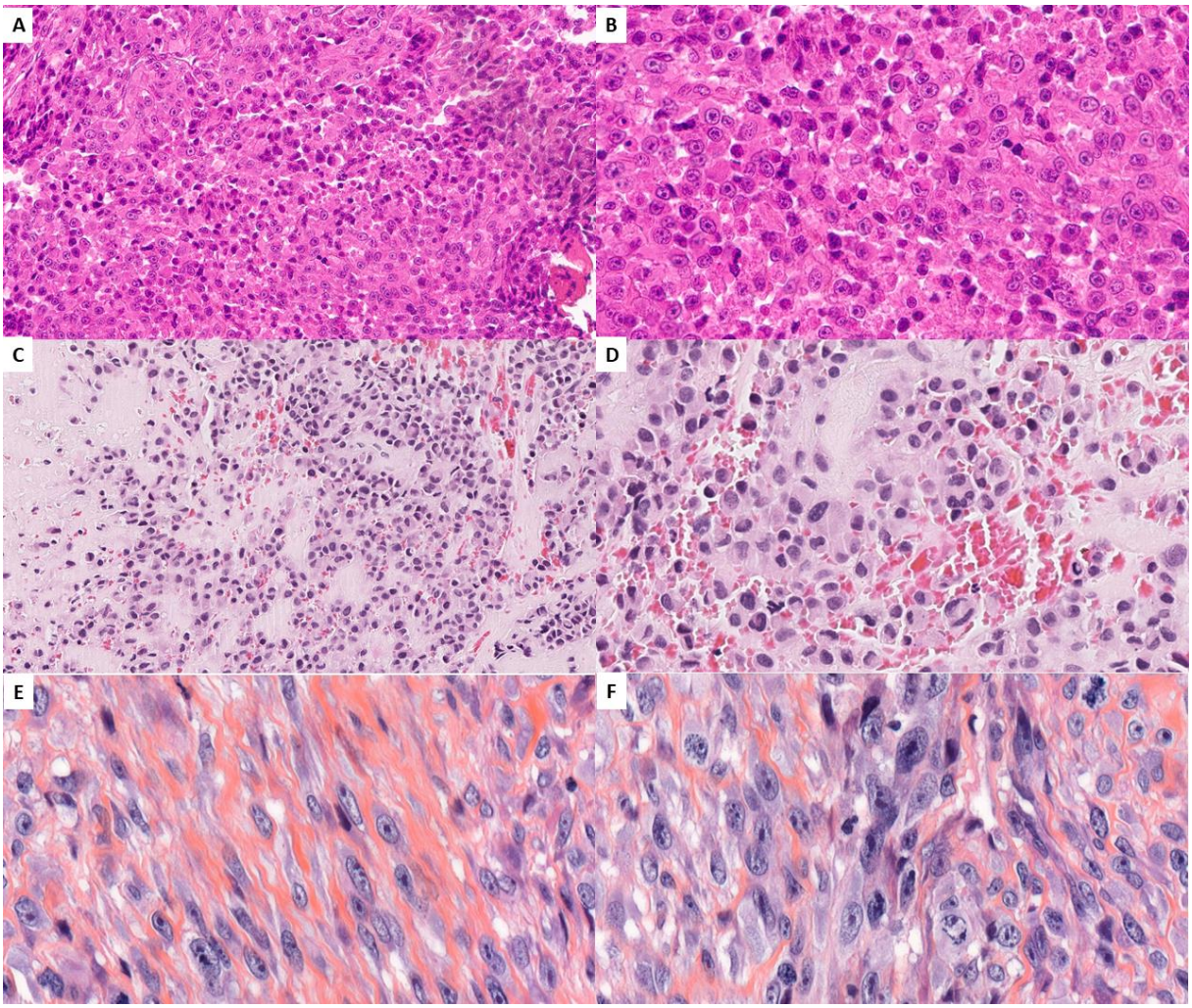

Figure 2

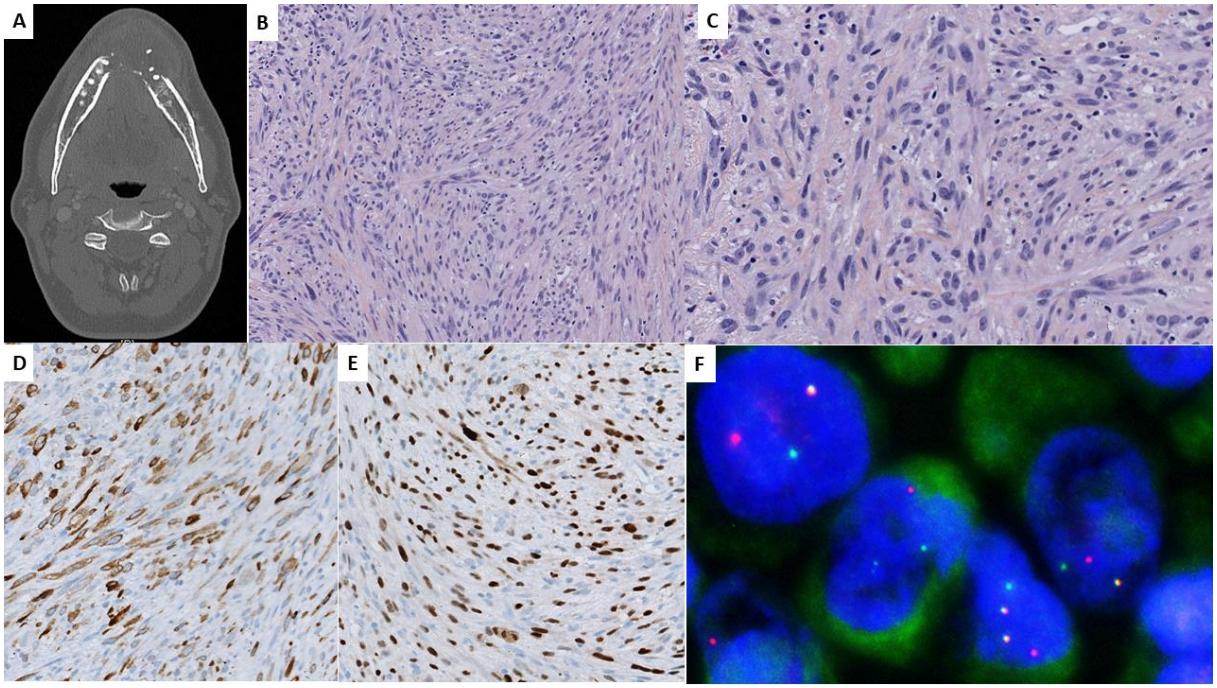

Figure 3

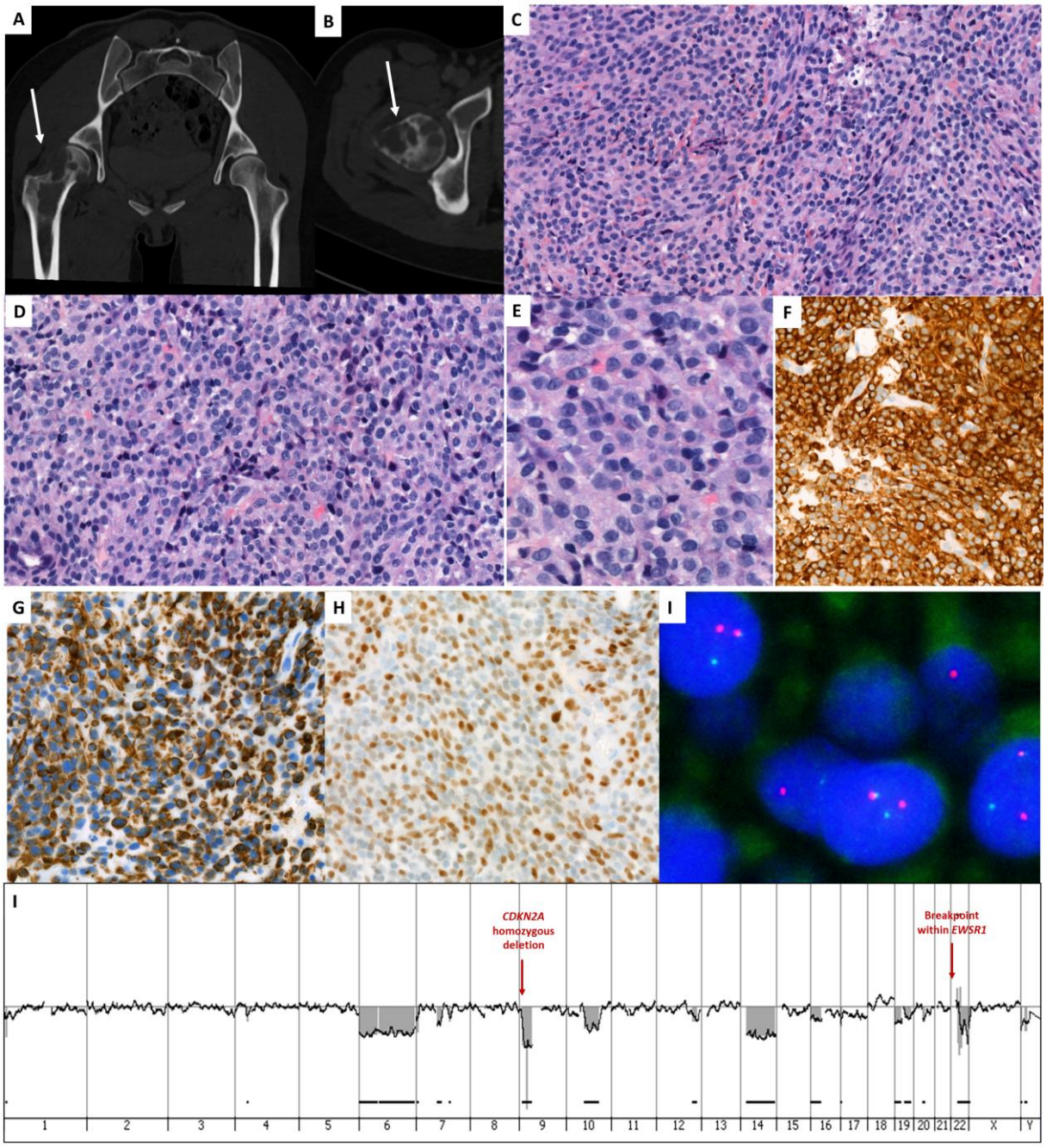
A
B
C
D
E
F
G
H
I
I
CDKN2A
homozygous
deletion
Breakpoint
within EWSR1
1
2
3
4
5
6
7
8
9
10
11
12
13
14
15
16
17
18
19
20
21
22
X
Y

Figure 4

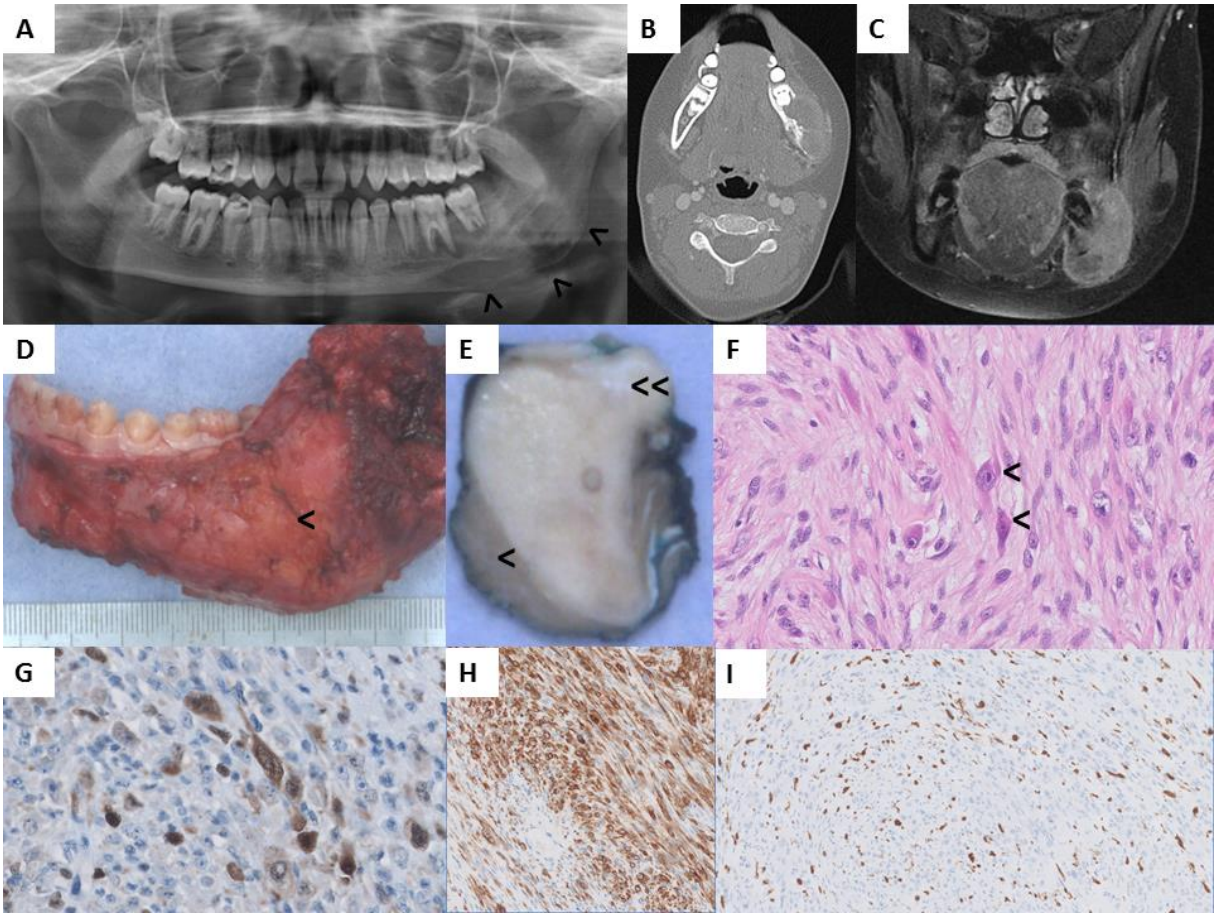

Figure 5